CHIN. PHYS. LETT. Vol. 37, No. 3 (2020) 036101

Atomic Mixing Induced by Ion Irradiation of V/Cu Multilayers *

Yan-Bin Sheng(盛彦斌)[1**], Hong-Peng Zhang(张宏鹏)[1], Tie-Long Shen(申铁龙)[1], Kong-Fang Wei(魏孔芳)[1], Long Kang(康龙)[1], Rui Liu(刘瑞)[2], Tong-Min Zhang(张桐民)[1], Bing-Sheng Li(李炳生)[3**]

[1]*Institute of Modern Physics, Chinese Academy of Sciences, Lanzhou 730000*
[2]*Key Laboratory of Materials Physics, Institute of Solid State Physics, Chinese Academy of Sciences, Hefei 230031*
[3]*State Key Laboratory for Environment-Friendly Energy Materials, Southwest University of Science and Technology, Mianyang 621010*

(Received 2 December 2019)

Bulk Cu/V multilayers simultaneously possess high strength and excellent radiation resistance thanks to their high density of interfaces. Irradiation-induced atomic mixing of Cu/V multilayers has been less investigated. Here, we investigate the ion irradiation of bulk Cu/V multilayers exposed to H_2^+ or He^+ ions at 350°C. The microstructure and elemental distribution are investigated by transmission electron microscopy and energy dispersive x-ray spectroscopy. Facetted bubbles and atomic mixing are observed after ion irradiation. The possible mechanisms of irradiation-induced atomic mixing are discussed.

PACS: 61.66.Dk, 61.72.−y, 61.80.Jh, 61.82.Bg DOI: 10.1088/0256-307X/37/3/036101

In nuclear radiation surroundings, structural materials suffer severe damage due to neutrons and energetic particles. The interactions between energetic projectile particles and target atoms of structural materials lead to atomic displacement damage, such as vacancies, interstitials and their agglomerations in the form of point defects, dislocation loops and voids, which will lead to dimensional instability and performance degradation.[1−7] Therefore, it is important to design structural materials with excellent radiation resistance to develop advanced nuclear reactors in the future.

To develop new structural materials, nanoscale metallic multilayers have attracted a great deal of attention from researchers because grain boundaries and hetero-interfaces can act as effective sinks for radiation-induced lattice defects, resulting in materials with self-repairing capabilities.[8−15] In particular, hetero-interfaces have unique properties, such as materials with different lattice mismatches and chemical bonds, leading to the construction of different interfaces in both physical and chemical ways. In addition, changing constituent materials and layer thickness can modify the mechanical and radiation resistance properties. Up to date, systems of metallic multilayers with FCC/BCC interfaces (Cu/Nb, Cu/V, Cu/Mo, Cu/W), FCC/FCC interfaces (Cu/Ni, Cu/Co, Ag/Ni) and BCC/BCC interfaces (Fe/W) have been developed.[16−21] Interfacial structures can decide microstructural evolution and mechanical properties under He^+ ion irradiation. Compared to the FCC/FCC and BCC/BCC interfaces, FCC/BCC incoherent interfaces with high positive enthalpy of mixing ($H_{\rm mix}$) generally exhibit more excellent radiation resistance. For example, it has been reported that immiscible Cu/Nb nanolayers with a layer thickness of a few nm have an extremely resistant ability against He^+ ion irradiation induced intermixing.[16,17] Meanwhile, He bubbles are seldom observed in Cu/Nb nanolayers with thickness of 2.5 nm. Demkowicz *et al.* used molecular dynamics simulations to confirm that at the Cu/Nb interface, two types of Kurdjumov–Sachs (K-S) orientation relationships can be changed by trapping a vacancy or an interstitial, and form extended jogs.[22] This phenomenon leads to the Cu/Nb interface effective acting as sinks for radiation-induced defects. Similarly, Fu *et al.* studied the effects of He^+ ion irradiation into C/V nanolayers with varying thickness from 1 to 200 nm, and confirmed that the magnitude of radiation hardening decreases with decreasing individual layer thickness, and radiation hardening is almost negligible when thickness is less than 2.5 nm.[18] In their study, Cu/V interface possesses chemical stability under 50 keV He^+ ion irradiation to a fluence of 6×10^{16} ions/cm^2 at room temperature (RT). However, there is also a report that ion beam mixing can be achieved in Cu/Fe nanolayers with a high positive $H_{\rm mix}$. In comparison with many reports of He^+ ion irradiation of metallic multilayers with nanoscale at RT, He^+ ion irradiation at elevated temperatures is more meaningful during structural materials used in nuclear radiation surroundings. In this Letter, we report atomic mixing of Cu/V nanolayers under He^+ or H_2^+ ion irradiation at 350℃, which is the surrounding temperature of the structural materials used in the pressurized water reactor. In addition, most of the studied metallic multilayers with nanoscale are fabricated by dc or rf magnetron sputtering in a high-vacuum system. However, fabrication of nanolayered composites in the bulk form by means of magnetron sputtering is very hard and we cannot use it for engineering applications. Recently, an accumulative roll bonding (ARB) was developed to fabricate bulk Cu/Nb nanolayers.[23] The bulk Cu/Nb nanolayers fabricated by ARB have excellent radiation resistance, high strength and thermal stability simul-

*Supported by the National Natural Science Foundation of China (Grant No. U1832133).
**Corresponding author. Email: Shengyb@impcas.ac.cn; libingshengmvp@163.com

taneously. Zeng *et al.* developed cross accumulative roll bonding (CARB) to fabricate nanolayered Cu/V composites.[24] The CARB process contains multiple cycles of cleaning, stacking, roll bonding and cutting. Meanwhile, a process with a sample rotated by 90° is added between every two roll-bonding cycles during CARB process. For the detailed description of CARB process, one can see Ref. [24]. Cu and V-based alloys are of important structural materials used in nuclear fusion reactors. In this study, bulk nanolayered Cu/V composites fabricated by CARB process are irradiated by hydrogen or helium ions. To explore the microstructural and chemical instability after ion irradiation, the irradiated samples are investigated by cross-sectional transmission electron microscopy (XTEM) and scanning transmission electron microscopy (STEM), as well as energy dispersive x-ray spectroscopy (EDX).

In our experiment, Bulk Cu/V multilayers with each Cu and V layer thicknesses varying from 20 to 200 nm were fabricated by the CARB process. Bulk Cu/V multilayers were irradiated at 350℃ by 130 keV He^+ ions with two different fluences of 1.1×10^{17} ions/cm^2 and 2.8×10^{17} ions/cm^2, or by 160 keV H_2^+ ions with a fluence of 5×10^{16} ions/cm^2 separately. The irradiation experiments were performed at a 320 kV high-voltage platform in the Institute of Modern Physics, Chinese Academy of Sciences. Beam scanning was carried out to achieve a uniform irradiation with an area of 16×17 mm^2, while the size of the sample is 10×10 mm^2, to ensure the entire sample surface irradiated. The beam flux during H_2^+ and He^+ ion irradiation were 2.5×10^{13} and 3.6×10^{13} ions/cm^2·s. The increase in sample temperature by ion irradiation, ΔT, can be estimated by[25]

$$\Delta T = \frac{2J}{k_{\mathrm{T}}} \left(\frac{k_{\mathrm{T}} t}{\rho C_{\mathrm{T}}} \right)^{1/2},$$

where J is beam power density in units of W/cm^2, k_{T} is thermal conductance in units of W/cm·K, t is beam time, ρ is density in units of g/cm^3, and C_{T} is specific heat in units of J/g·K. For simplicity, according to the He irradiation condition, ΔT can be estimated to be nearly from 14.6℃ to 23.4℃ for Cu films.

The microstructure of bulk CARB Cu/V multilayers was investigated by a 200 kV Tecnai G20 microscopy with a point resolution of 0.19 nm. The XTEM sample was prepared by a Hitachi 2000 focused ion beam (FIB) system. Before cutting process, the irradiated surface was protected with a deposited tungsten layer. Irradiation-induced bubbles were imaged using under-focused and over-focused conditions. The STEM and the EDX analysis for identifying the elemental composition and the interface integrity of the irradiated samples were carried out by the Tecnai G20 with a STEM high angle annular dark field (HAADF) detector and an EDX detector of Oxford instruments with a spatial resolution of about 1 nm.

The bright-field XTEM micrographs shown in Fig. 1 represent the microstructure of the CARB Cu/V multilayers. It can be seen that the as-fabricated bulk Cu/V multilayers exhibit a continuous nanolayered structure with different contrasts of Cu and V layers. The Cu/V interfaces were relatively sharp. The thickness of each layer of Cu and V, measured from the XTEM image, ranges from 20 to 200 nm. In the nanolayer, dislocation arrays and isolated dislocation loops exhibited black contrast were observed and indicated by arrows. It should be noted that not all the observed black contrast is attributed to dislocation and dislocation loops. The curve of nanolayers can also produce black contrast that can be ruled out through tilting XTEM samples. The black contrast due to the curve of nanolayers will move when the sample is tilted. These observed dislocations and the curve of nanolayers were introduced during CARB process. Besides these large black contrasts, some black spots were observed in the Cu and V nanolayers. These black spots were probably formed due to Ga ion collision during the FIB process.

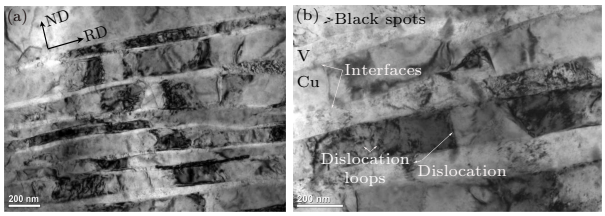

Fig. 1. [(a), (b)] Typical bright-field XTEM images of the as-fabricated bulk CARB Cu/V multilayers. Bright contrast is V layer and dark contrast is the Cu layer. Some lattice defects are indicated by arrows. The normal direction (ND) and the rolling direction (RD) are noted.

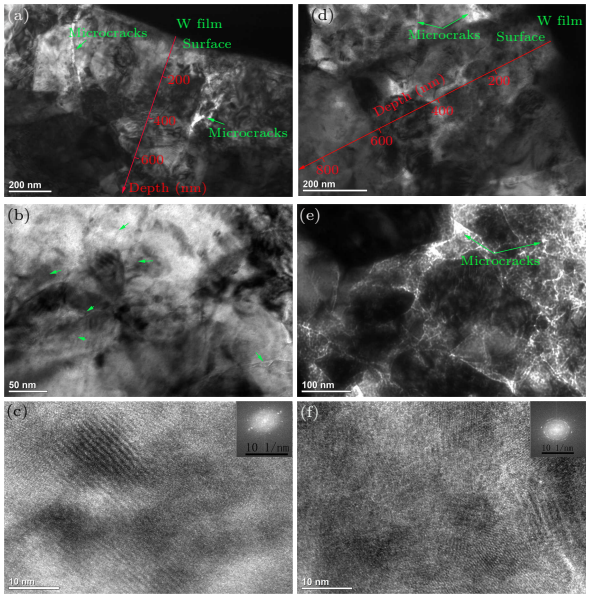

Fig. 2. Bright-filed XTEM images of the bulk Cu/V multilayers irradiated with 130 keV He^+ ions (a) to a fluence of 1.1×10^{17} ions/cm^2 at 350℃, (b) the magnified image of (a) showing bubbles indicated by green arrows, (c) HRTEM image of (a) showing polycrystalline in the irradiated layer; (d) to a fluence of 2.8×10^{17} ions/cm^2 at 350℃, (e) the magnified image of (d) showing microcracks indicated by green arrows, (f) HRTEM image of (a) showing polycrystalline and slight amorphization in the irradiated layer.

Figure 2 presents an overview of the damaged region of the sample irradiated with He^+ ions. For the sample irradiated with He^+ ions to a fluence of 1.1×10^{17} ions/cm^2, microcracks and dislocation loops were observed in the irradiated layer. The formation of microcracks is due to accumulation of facetted bubbles that were formed through the growth of He atoms and vacancies. Facetted bubbles were usually observed in metal alloys irradiated with He atoms at elevated temperature ($\sim 0.3T_m$).[26] The high resolution transmission electron microscopy (HRTEM) image shows polycrystalline in the irradiated layer, as confirmed by electron diffraction pattern shown in the inset of Fig. 2(c). For the sample irradiated with He ions to a fluence of 2.8×10^{17} ions/cm^2, the damaged layer converts to be porous due to dense bubbles formed, as shown in Fig. 2(e). The HRTEM image also shows polycrystalline and even slight amorphization in the damaged layer, as confirmed by electron diffraction pattern shown in the inset of Fig. 2(f).

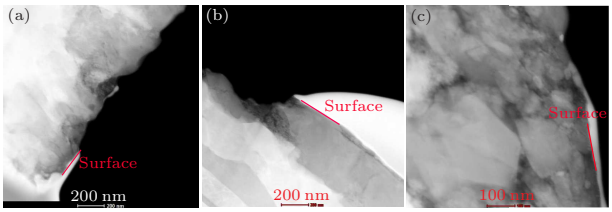

Fig. 3. HAADF-STEM images showing the bulk Cu/V multilayers irradiated with (a) 160 keV H_2^+ ions to a fluence of 5×10^{16} ions/cm^2 at 350℃, (b) 130 keV He^+ ions to a fluence of 1.1×10^{17} ions/cm^2 at 350℃, (c) 130 keV He^+ ions to a fluence of 2.8×10^{17} ions/cm^2 at 350℃.

Figure 3 presents the HAADF-STEM images of the Cu/V multilayers irradiated with H_2^+ or He^+ ions. In addition, the simulated damaged and H or He deposition profiles provided by the SRIM-2008 program and elemental Cu and V detected by EDX through linear scan are given in Fig. 4. In HAADF-STEM mode, the larger mass number z, the brighter contrast can be observed. The mass numbers of Cu and V are 64 and 51, respectively. Therefore, the V layer exhibits grey contrast and the Cu layer exhibits bright contrast. For the sample irradiated with He^+ ions to a fluence of 1.1×10^{17} ions/cm^2, the HAADF-STEM image shown in Fig. 3(a) displays the first irradiated layer that belongs to the V layer. Linear scan was performed to measure the distribution of elemental Cu and V. We can obtain the thickness of the V layer up to 300 nm. This result is larger than the as-fabricated bulk Cu/V multilayers shown in Fig. 1. The increase in the thickness can be attributed to He bubbles-induced volume swelling, which is confirmed by bright field XTEM image showing micro-cracks and porous structures in the V layer. More importantly, slight atomic mixing located at the maximum He-induced damage was clearly observed by EDX measurement, as shown in Fig. 4(b). For the sample irradiated with He^+ ions to a fluence of 2.8×10^{17} ions/cm^2, the HAADF-STEM image shown in Fig. 3(c) displays the first irradiated layer that is difficultly distinguished due to heavy irradiation disorder. The Cu/V interface cannot be clearly distinguished, instead of many grains with different sizes formed in the irradiated layer. The bright field image shown in Fig. 2(e) presents that many micro-cracks exist among the grains. A linear scan from the sample surface to a depth of 800 nm shows atomic mixing in the near surface region, as shown in Fig. 4(c). Point measurement was performed to check the elements between two grains. The measured data are shown in Fig. 4(d). It can be seen that elemental C, O, V, Cu and Ga exist simultaneously. The atomic percentages of C, O, V, Fe, Cu and Ga are 35.4 + 0.6%, 32.9 + 0.8%, 17.8 + 0.5%, 7.0 + 0.4%, 5.5 + 0.4% and 0.2+ 0.1%, respectively. The existence of elemental C and O is due to the XTEM sample contamination in air. Elemental Fe is introduced during the CARB progress, and elemental Ga is due to the XTEM sample fabricated by Ga^+ ions. To investigate the influence of mass atoms, a hydrogen irradiation experiment was performed. The sample was irradiated with 160 keV H_2^+ ions to a fluence of 5×10^{16} ions/cm^2 at 350℃. The HAADF-STEM image is shown in Fig. 3(a) and a linear scan from the sample to a depth of 650 nm displays Cu–V atoms mixed in the irradiated layer, as shown in Fig. 4(a).

There are three main processes that can describe the atomic transport in multilayers: (1) thermal diffusion, (2) irradiation enhanced thermal diffusion, and (3) athermal irradiation mixing (ballistic mixing).[27] During ion irradiation, the atomic mixing can be attributed to the combination action of these three processes. The process of atomic mixing can be described by Fick's law, $J = -D(\frac{\partial C}{\partial x})$, where J is the flux, D is the diffusion coefficient, and C is the concentration. The atomic transport can be attributed to different diffusion coefficients. Thermal diffusion can be described by a diffusion coefficient of the form $D_{\rm th} = C_{\rm def} D_{\rm def}$, where $C_{\rm def}$ is the concentration of the defect responsible for diffusion. The diffusion coefficient of the defect is expressed by $D_{\rm def} = \frac{1}{6} a^2 \nu \exp(-E/kT)$, where a is the jump distance, ν is the vibration frequency, and E is the migration energy of the defect during diffusion. The thermal diffusion $C_{\rm def}$ is expressed by $C_{\rm def}^{\rm th} = \exp(-E_{\rm f}/kT)$, where $E_{\rm f}$ is the formation energy of the defect. For the case of irradiation enhanced diffusion, $C_{\rm def}$ can be described by $C_{\rm def} = C_{\rm def}^{\rm th} + C_{\rm def}^{\rm irr}$, where $C_{\rm def}^{\rm irr}$ is the steady-state concentration of defects under irradiation. For the present case, the ballistic mixing is independent of temperature and is described by $D_{\rm bal} = \frac{1}{6} \Gamma a^2$, where Γ is the displacement rate (dpa/s) and a is the average distance atoms displaced in the collision cascade.

Under ion irradiation, the above-mentioned three processes are active simultaneously. The atomic mixing can be described by a combination of irradiation enhanced and thermal processes, and is given by $D_{\rm eff} = D_{\rm th} + D_{\rm bal} = \frac{1}{6} a^2 \nu \exp(-E/kT) \exp(-E_{\rm f}/kT) + \frac{1}{6} \Gamma a^2$, where $D_{\rm eff}$ is the total effective diffusion coefficient in the periphery of Cu/V interface.

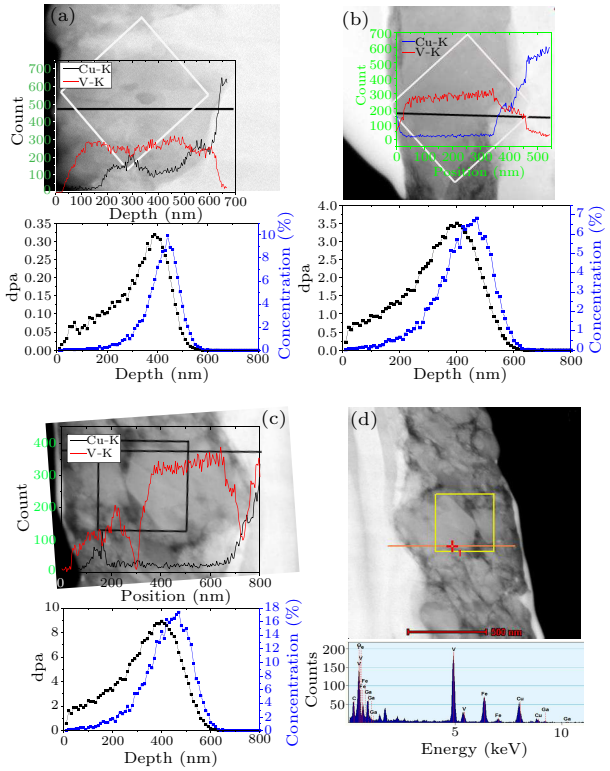

Fig. 4. HAADF-STEM images of the bulk Cu/V multilayers irradiated with (a) 160 keV H_2^+ ions to a fluence of 5×10^{16} ions/cm^2 at 350℃, (b) 130 keV He^+ ions to a fluence of 1.1×10^{17} ions/cm^2 at 350℃, (c) and (d) 130 keV He^+ ions to a fluence of 2.8×10^{17} ions/cm^2 at 350℃. The linear scanning by EDX showing V–K and Cu–K counts is overlaid on the corresponding HAADF-STEM image. In addition, the depth profiles of irradiation damage and H or He concentration induced by 160 keV H_2^+ ion irradiation (b) and (c) 130 keV He^+ ion irradiation are simulated by the stopping and range of ions in matter (SRIM) computer program based on the Monte Carlo method in $Cu_{50}V_{50}$ composites. The threshold displacement energy for Cu and V are 29 and 39 eV, respectively.[28]

As mentioned earlier, atomic collision cascades can increase the local redistribution of components. However, chemical driving force (thermodynamic effect) in Cu/V immiscible systems with strong positive mixing enthalpy of 5 kJ/mol can separate Cu and V atoms automatically.[29] For the case of He irradiation at RT, atomic mixing does not occur, even the He irradiation dose up to 12 dpa. However, in the present He irradiation at 350℃ to a dose of 3.5 dpa, we have observed atomic mixing in the peak He damage. Some V atoms under the influence of ion irradiation and thermal effect diffuse into the Cu layer. In particular, in the H_2^+ ions irradiated at 350℃ to a dose of 0.32 dpa, the Cu and V layers are completely mixed in the irradiated region. It should be noted why the completely mixed Cu and V layers occurred in the Cu/V multilayers irradiated with H_2^+ ions to a dose of 0.32 dpa, but not in the He^+ ion to a dose of 3.5 dpa. If the irradiation enhanced diffusion makes more role of atomic mixing, the completely mixed Cu and V layers should occur in the He^+ ion irradiation. However, we observe the inverse phenomenon. We are sure that the thermal diffusion plays more role of atomic mixing. Because the H_2^+ and He^+ ion irradiations were performed at the same temperature of 350℃, the observed thermal diffusion is not only surrounding temperature, but also inelastic energy loss of H_2^+ ion irradiation. The ratio of electronic energy loss to nuclear energy loss is 387 for the 160 keV H_2^+ ion irradiation, while it is 77.5 for the 130 keV He^+ ion irradiation. Therefore, the electronic energy loss is much higher than nuclear energy loss in the H_2^+ ion irradiation. It is well recognized that a thermal spike effect can explain the phenomenon of electron energy loss. According to the thermal spike mode, rapid energy transfer through electron-phone coupling makes the system abnormally excited, and the region around the ion track becomes heated to a very high temperature within a short time scale and then quenched on a picosecond scale. Therefore, for the case of H_2^+ ion irradiation, extra heat was introduced by electron energy loss, which can account for the completely mixed Cu and V nanolayers. Dong *et al.* reported that Cu/W multilayers with each 24 nm thickness can be mixed at between Cu and W nanolayers, due to ballistic effect of 6.4 MeV Xe^{20+} ion irradiation to a fluence of 1.5×10^{15} ions/cm^2 at RT.[30] However, the Cu/W multilayers with each thickness of 18 nm or less, no mixed interface was observed after Xe^{20+} ion irradiation. The decrease in thickness of nanolayers can enhance irradiation resistance. Chemical disorder at between Cu and V nanolayer can easily occur due to interface acting as efficient sinks for irradiation-induced defects. For the case of He^+ ion irradiation to a fluence of 1.1×10^{17} ions/cm^2, many V and Cu self-interstitials are formed. These V self-interstitials migrate toward the Cu layer, resulting in the formation of vacancy sites behind that can absorb Cu self-interstitials. Therefore, the mixed interface was observed in the Cu/V multilayers irradiated with He^+ ions to a fluence of 1.1×10^{17} ions/cm^2. However, it cannot exclude the intermixing between immiscible metals under severe deformation conditions during the CARB process. Wei *et al.* investigated deformation-induced interfacial transition zone in Cu/V nanolamellar fabricated by CARB, and found a deformation-induced interfacial transition zone with a thickness of about 5 nm in Cu/V multilayers.[21] Dislocation activities near the bimetal interfaces can explain the intermixing phenomenon. In the case of He^+ ions to a fluence of 1.1×10^{17} ions/cm^2, the thickness of the intermixing is about 50 nm, which is larger than the reported result of the as-fabricated material. The width of the mixed interface increases with the increase in He fluence. Hence, the Cu and V nanolayers were mixed during He^+ ion irradiation to a fluence of 2.8×10^{17} ions/cm^2. Further investigation is necessarily performed on the intensity of the mixed interface with irradiation fluence. Because of the present studied bulk Cu/V multiplayers with thickness over 20 nm, the role of interfaces acting as sinks for irradiation-induced defects is less significant. It is necessary to investigate the irradiation-induced atomic mixing in bulk Cu/V multiplayers with thickness of only few nm

at elevated temperature.

In conclusion, we have investigated bulk Cu/V multilayers for each layer of Cu and V in thicknesses varying from 20 to 200 nm fabricated by the CARB method, which are irradiated with H_2^+ or He^+ ions at 350℃. Facetted bubbles and microcracks are formed in the irradiated layer. An irradiation-induced atomic mixing is observed. This phenomenon can be explained by a combination of irradiation enhanced and thermal processes.

References

[1] Zinkle S J and Was G S 2013 *Acta Mater.* **61** 735
[2] Wang K, Bannister M E, Meyer F W, Parish C M 2017 *Acta Mater.* **124** 556
[3] Wang K, Dai Y and Spatig P 2016 *J. Nucl. Mater.* **468** 246
[4] Li B S, Wang Z G, Shen T L et al 2019 *Chin. Phys. Lett.* **36** 046104
[5] Fang X S, Shen T L, Cui M H et al 2017 *Chin. Phys. Lett.* **34** 116102
[6] Li Y F, Shen T L, Gao X et al 2014 *Chin. Phys. Lett.* **31** 036101
[7] Klueh R L, Gelles D S, Jitsukawa S, Kimura A, Odette G R, Schaaf van der B and Victoria M 2002 *J. Nucl. Mater.* **307–311** 455
[8] Zhang J Y, Wang Y Q, Liang X Q, Zeng F L, Liu G and Sun J 2015 *Acta Mater.* **92** 140
[9] Zhu H L, Qin M J, Aughterson R, Wei T, Lumpkin G, Ma Y and Li H J 2019 *Acta Mater.* **172** 72
[10] Zhang H X, Ren F, Wang Y Q, Hong M Q, Xiao X H, Qin W J and Jiang C Z 2015 *J. Nucl. Mater.* **467** 537
[11] Han W Z, Mara N A, Wang Y Q, Misra A and Demkowicz M J 2014 *J. Nucl. Mater.* **452** 57
[12] Han W Z, Demkowicz M J, Mara N A, Fu E G, Sinha S, Rollett A D, Wang Y Q, Carpenter J S, Beyerlein I J and Misra A 2013 *Adv. Mater.* **23** 6975
[13] Hong M Q, Ren F, Wang Y Q, Zhang H X, Xiao X H, Fu D J, Yang B and Jiang C Z 2015 *Nucl. Instrum. Methods Phys. Res. Sect. B* **342** 137
[14] Chen H C, Zhan X Z, Liu X, Hai Y, Xu J P, Zhu T and Yin W 2019 *Appl. Surf. Sci.* **486** 274
[15] Zhang X H, Hattar K, Chen Y X, Shao L, Li J, Sun C, Yu K Y, Li N, Taheri M L, Wang H Y, Wang J and Nastasi M 2018 *Prog. Mater. Sci.* **96** 217
[16] Zhang X, Li N, Anderoglu O, Wang H, Seadener J G, Hochbouer T, Misra A and Hoagland R G 2007 *Nucl. Instrum. Methods Phys. Res. Sect. B* **261** 1129
[17] Zhernenkov M, Jablin M S, Misra A, Nastasi M, Wang Y, Demkowicz M J, Baldwin J K and Majewski J 2011 *Appl. Phys. Lett.* **98** 241913
[18] Fu E G, Misra A, Wang H, Shao L and Zhang X 2010 *J. Nucl. Mater.* **407** 178
[19] Wang M, Beyerlein I J, Zhang J and Han W Z 2018 *Acta Mater.* **160** 211
[20] Callisti M, Karlik M and Tolcar T 2016 *J. Nucl. Mater.* **473** 18
[21] Wei S Y, Zhang L F, Zheng S J, Wang X P and Wang J W 2019 *Scr. Mater.* **159** 104
[22] Demkowicz M J, Hoagland R G, Uberuaga B P and Misra A 2011 *Phys. Rev. B* **84** 104102
[23] Zheng S, Beyerleim I J, Carpenter J S, Kang K, Wang J, Han W and Mara N A 2013 *Nat. Commun.* **4** 1696
[24] Zeng L F, Gao R, Xie Z M, Miao S, Fang Q F, Wang X P, Zhang T and Liu C S 2017 *Sci. Rep.* **7** 40742
[25] Nastasi M, Mayer J and Hirvonen J K 1996 *Ion-Solid Interactions: Fundamentals and Applications* (New York: Cambridge University Press)
[26] Li B, Wang Z, Wei K, Shen T, Yao C, Zhang H, Sheng Y, Lu X, Xiong A and Han W 2019 *Fusion Eng. Deg.* **142** 6
[27] Motta A T, Jr Paesano A, Birtcher R C, Bruckmann M E, Teixeira S R and Amaral L 1999 *J. Appl. Phys.* **85** 7146
[28] Ziegler J F, Ziegler M D and Biersack J P 2010 *Nucl. Instrum. Methods Phys. Res. Sect. B* **268** 1818
[29] Boer, F R, Mattens W C M, Miedema A R and Niessen A K 1989 Cohesion in Metel: Transition Metal Alloys (Amsterdam: North-Holland)
[30] Dong L, Zhang H X, Amekura H, Ren F, Chettch A, Hong M Q, Qin W J, Tang J, Hu L L, Wang H and Jiang C Z 2017 *J. Nucl. Mater.* **497** 117